

# High temperature oxidation and mechanical behavior of $\beta$ 21s and Ti6242S Ti-based alloys

<sup>1</sup>Aurelie Vande Put\*, <sup>1</sup>Carole Thouron, <sup>2</sup>Philippe Emile, <sup>2</sup>Raphaëlle Peraldi, <sup>2</sup>Benjamin Dod, <sup>1</sup>Daniel Monceau

<sup>1</sup>CIRIMAT, Université de Toulouse, CNRS, INP- ENSIACET 4 allée Emile Monso - BP44362, 31030 Toulouse cedex 4 - France

<sup>2</sup>Airbus Operations S.A.S., 316 route de Bayonne, 31060 Toulouse, France

\*aurelie.vandeput@ensiacet.fr

## **Abstract**

Aircraft industry always looks for higher in-service temperatures and lighter structures. With a high specific strength, Ti-based alloys are good candidates for such applications. However, when exposed to oxidizing environments at high temperatures, they undergo large oxygen dissolution while forming an oxide scale, which can greatly affect their mechanical properties. Then, evaluating the oxidation resistance and mechanical behavior of such alloys is essential. In this aim, long term oxidation tests were performed under laboratory air between 500 °C and 625 °C on two Ti-based alloys:  $\beta$ 21s, exhibiting a fully  $\beta$  microstructure supposed to dissolve lower amount of oxygen and nitrogen, and Ti6242S, with an  $\alpha/\beta$  microstructure. The oxidized samples were characterized using XRD, Raman spectroscopy, SEM-EDS and micro-durometer. As for the mechanical behavior, tensile tests were performed at room temperature on not aged and on oxidized samples. While larger mass variations were obtained at 500 and 560 °C and up to 997 h at 625 °C for  $\beta$ 21s, its mass variations became lower than those of Ti6242S for longer durations at 625 °C. Nevertheless,  $\beta$ 21s exhibited thicker micro-hardness affected depths and underwent larger mechanical property modifications compared to Ti6242S.

## **1. Introduction**

For many years, aircraft industry has been looking for higher in-service temperatures and lighter structures, needs that become even more marked today because of environmental norms. Ti-based alloys are good materials for such applications, because of their high specific strength [1,2]. Nevertheless, they undergo large oxygen (and nitrogen) dissolution in the same time as they form an oxide scale when they are exposed to oxidizing environments at high temperatures [3,4]. This oxygen diffusion, because it can greatly affect their mechanical properties [5-7], limits the in-service temperature of such materials. It is then essential to

evaluate the oxidation resistance and mechanical behavior of oxidized Ti-based alloys. To do so, long term oxidation tests were performed under laboratory air between 500 °C and 625 °C on two Ti-based alloys:  $\beta$ 21s and Ti6242S alloys. Few oxidized samples were analysed to characterize the formed oxide scale and the oxygen-rich metallic layer underneath. Others were mechanically tested and compared to not aged samples in order to evaluate the impact of environment on the resistance to tensile stresses.

## 2. Materials and experiments

### Materials

Two Ti-based alloys were studied: Ti6242S and  $\beta$ 21s in the form of sheet material. Energy dispersive X-ray spectroscopy (EDS) was used to determine the alloy composition in heavy elements while instrumental gas analysis (IGA) and glow discharge mass spectrometry (GDMS) analyses were realized to measure light element contents by Evans analytical Group SAS (Tournefeuille, France). Obtained compositions are reported Table 1. The alloys contained similar oxygen amounts (about 1000 ppm). The largest differences were noticed for C and N ;  $\beta$ 21s alloy was richer in nitrogen.

**Tableau 1: Chemical composition of Ti6242S and  $\beta$ 21s alloys**

	Main elements, by EDS, in wt.%								Others elements in ppmw
	Ti	Al	Sn	Zr	Mo	Nb	Si	Fe	
<b>Ti6242S</b>	Base	6.3	2.0	3.7	1.6	-	-	-	GDMS: 750Si, 270Fe, 13Cr, 25Ni, 360H IGA: 19C, 13N, 850O, 30H, <5S
<b><math>\beta</math>21s</b>	Base	3.2	-	-	14.5	2.6	0.4	~0.27	GDMS: 16Zr, 38Sn, 54Cr, 120Ni, 0.3Hf IGA: 160C, 140N, 1300O, 33H, <5S

Ti6242S alloy was hot rolled below  $\beta$  transus and duplex annealed as per AMS4919 (899°C/30min air cooling + 788°C/15 min air cooling) leading to an  $\alpha/\beta$  globular microstructure, see Figure 1.a.  $\beta$ 21s alloy was also hot rolled. However, as no solution annealing and ageing heat treatment was applied to precipitate the  $\alpha$ -phase, the alloy exhibited a fully  $\beta$  microstructure, see Figure 1.b, with a grain size of around 38  $\mu$ m (according to image analysis on chemically etched samples).

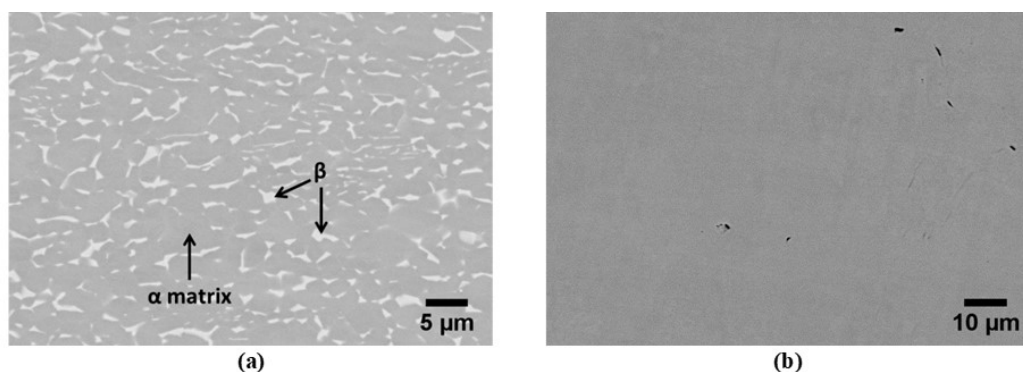


**Figure 1: Microstructure of as-received (a) Ti6242S and (b)  $\beta$ 21s alloys. SEM images in BSE mode.**

Two rolled sheets were available, 3.97 mm and 1.85 mm thick for Ti6242S and  $\beta$ 21s respectively. 19.7 x 19.7 mm squared specimens were cut from these sheets, and their surface was ground using P240 SiC paper before a cleaning in an ultrasonic bath of acetone and then of ethanol for the oxidation tests.

Tensile test specimens (flat specimens, 12.5 mm in width) were cut out from the sheets, 3.97 mm and 1.85 mm thick for Ti6242S and  $\beta$ 21s respectively. No polishing or grinding step was made so that the specimen surface remained in the as delivered condition. Prior to ageing and tensile test, specimens were cleaned in an ultrasonic bath of acetone and then of ethanol to be oxidized.

#### *Oxidation tests*

Samples were placed on ceramic bricks in Nabertherm N60/85HA and N120/85HA furnaces. Both alloys were oxidized 2958 h at 500, 560 and 650 °C under laboratory air. A Sartorius Genius (ME215-P) balance with an accuracy of 20  $\mu$ g was used for mass measurements before and after oxidation. Each recorded mass was the average of two weightings.

#### *Tensile tests*

Tensile tests were performed at room temperature according to EN2002-1, using a strain rate equal to 2 mm/min up to failure. For each alloy, three samples were oxidized before mechanical testing for 2958 h at 625 °C under laboratory air, with the squared specimens used for oxide scale and oxygen diffusion characterization. Their mechanical behavior was compared to the one of three unaged specimens of corresponding alloy.

#### *Characterization*

X-ray diffraction analyzes (XRD) were performed using a Seifert 3000TT apparatus with a copper anti-cathode ( $\lambda = 1.54056 \text{ \AA}$ ). Raw materials were analyzed using a theta-theta mode between 20 and 120 ° (2 $\theta$ ) with a step of 0.04 ° and an acquisition time of 3 s per step. Oxidized sample analyses were done between 20 and 80 ° (2 $\theta$ ) with a low incidence angle (between 2 and 8 °), a step of 0.05 ° and an acquisition time of 10 s per step.

Raman and fluorescence spectroscopy analyses were made using a Labram HR 800 spectrometer from Horiba Yvon Jobin, equipped with a confocal microscope. Spectra were recorded using a laser with a 532 nm line.

Cross-sections were made starting by a pre-coating with an epoxy resin to protect the oxide scale during the cut. The grinding and polishing sequence started with a P180 up to a P2400 SiC paper and finished using OPS.

SEM observations of the surface and cross-section of oxidized and reference samples were done with a LEO 435VP microscope using the secondary electron imaging mode (SE) or the backscattered electron imaging mode (BSE). EDS analyses were done with an IMIX system from PGT and quantification was based on real standards. To reach higher magnifications to observe the aged microstructures, a JSM-7800F FEG-SEM from JEOL was used while the fracture surface of the tensile specimens was performed with a FEI Quanta 600 microscope.

Vickers micro-hardness measurements were realised using a Buehler Omnimet 2100 serie with a 50 g diamond indent. To estimate the depth of the micro-hardness affected zone, the reference value was chosen as being the average value of micro-hardness measurements obtained in the non-affected zone, close to the bulk (imprints exhibiting an un-explained high value in the bulk were not considered to evaluate the reference value). Then, micro-hardness affected zone was evaluated as the depth where hardness was at least 25 Hv higher than the reference value.

### 3. Results

#### Oxidation tests

The net mass changes measured during long isothermal oxidation tests are presented on Figure 2. While both alloys underwent relatively small mass variations after 2958 h at 500 °C and 560 °C (inferior to 1 mg/cm<sup>2</sup>), mass variations became more marked during the exposition at 625 °C. Besides, alloy ranking was reversed between 625 °C and the lower oxidizing temperatures. At 500 °C and 560 °C,  $\beta$ 21s alloy exhibited larger mass changes compared to Ti6242S alloy (1.8 and 1.7 times larger than the one of Ti6242S at 500 and 560 °C respectively). At 625 °C,  $\beta$ 21s maintained a higher mass change than Ti6242S alloy up to 997 h. However, for longer durations at this temperature, the mass variation of Ti6242S alloy exceeded the one of  $\beta$ 21s alloy, and became 1.3 times larger than the one of  $\beta$ 21S at 2958 h.

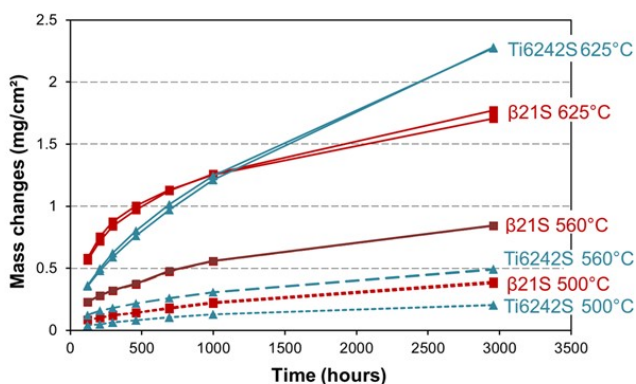


**Figure 2:** Net mass changes of Ti6242S and  $\beta$ 21s alloys oxidized under laboratory air.

XRD, Raman spectroscopy and fluorescence spectroscopy analyses were performed to determine the nature of the oxide scale. Figures 3 and 4 gather data obtained for both alloys oxidized 2958 h at 625 °C. At 500 °C, anatase TiO<sub>2</sub> was the main oxide detected on Ti6242S, with a small proportion of rutile, while rutile and anatase TiO<sub>2</sub> composed the oxide scale of Ti6242S exposed at 560 °C and 625 °C. As for  $\beta$ 21s, rutile and anatase TiO<sub>2</sub> composed the oxide scale, anatase being in greater proportion.  $\alpha$ -alumina was also detected on both alloys, but only after exposures at 625 °C.

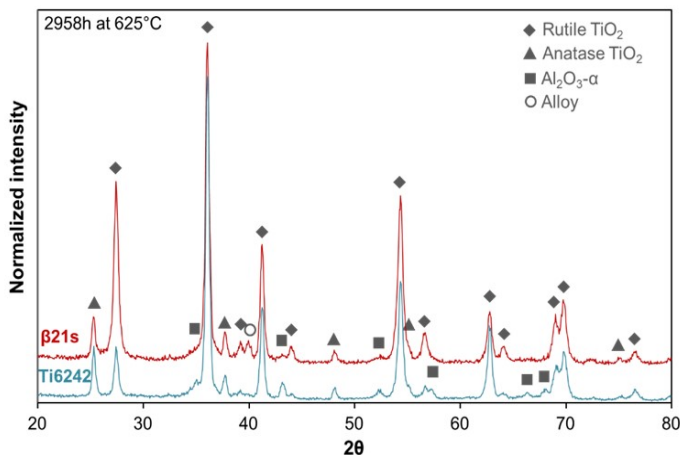


Figure 3: XRD of Ti6242S and  $\beta$ 21s alloys oxidized under laboratory air at 625 °C for 2958 h.

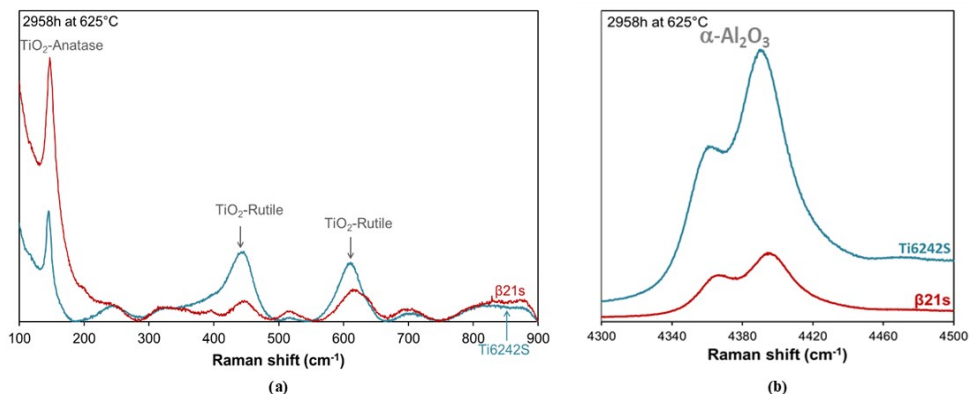
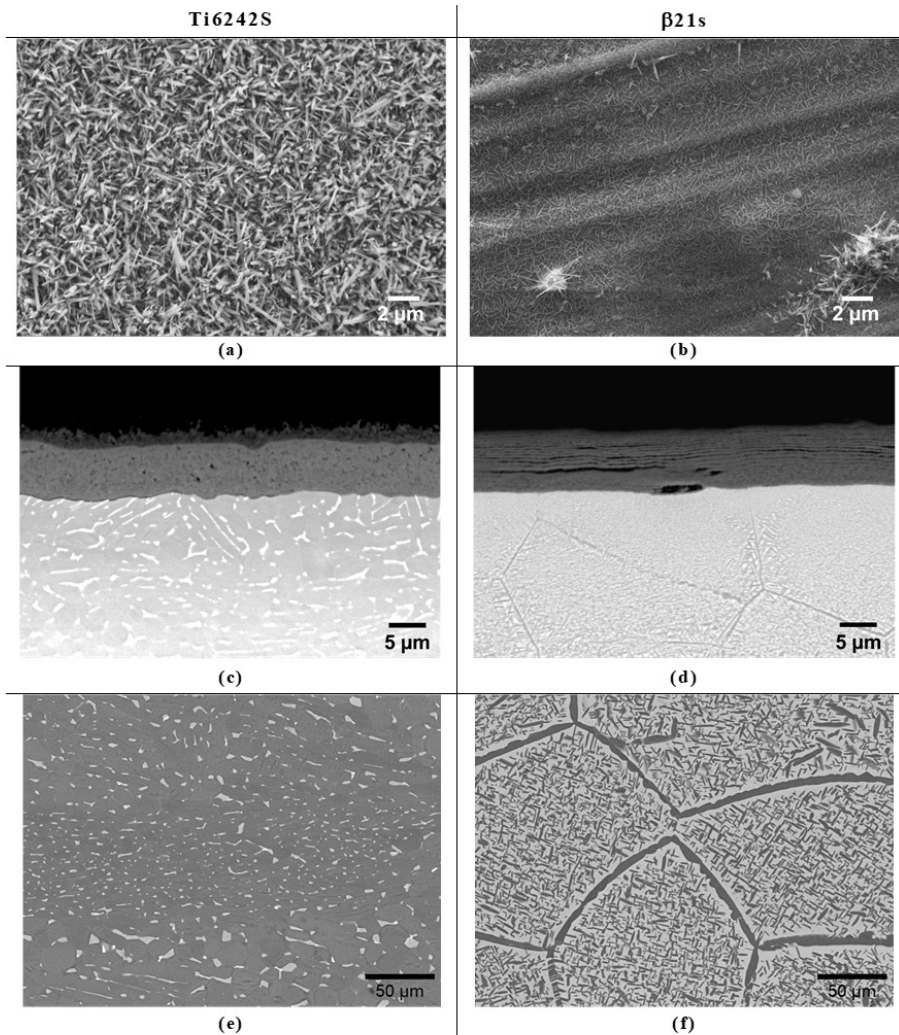


Figure 4: Raman spectra of Ti6242S and  $\beta$ 21s oxidized under laboratory air at 625 °C for 2958 h. (a) Raman domain, (b)  $\text{Cr}^{3+}$  fluorescence domain.

Regarding the oxide scale morphology, needle shaped oxides formed rapidly on Ti6242S, while such morphology started to become visible on  $\beta$ 21s surface much later, see Figure 5.a,b. Besides, the greater time and temperature were, the larger the amount of needle shaped oxides was. SEM observations of the oxide scale cross-sections pointed out another difference in terms of oxide scale morphology, Figure 5.c,d. After 2958 h of oxidation at 625 °C, Ti6242S alloy exhibited a relatively dense inner layer below an outer scale composed of needle shaped oxides. After a similar oxidation, a stratified oxide scale was present on  $\beta$ 21s alloy (each oxide layer being around 1  $\mu\text{m}$  thick, or less). EDS analysis revealed the external layer formed on Ti6242S was enriched in Al, while a small enrichment in Al was found on top of the oxide scale present on  $\beta$ 21s alloy. Finally, the dense part of the oxide scale formed on Ti6242S was around 10% thinner than the oxide scale of  $\beta$ 21s alloy.



**Figure 5:** (a) and (b) Oxide scale surface, (c) and (d) oxide scale cross-section and (e) and (f) bulk microstructure of (a, c, e) Ti6242S and (b, d, f) β21s oxidized under laboratory air at 625 °C for 2958 h. SEM images in (a, b) SE mode and (c, d) BSE mode. (e, f) FEG-SEM images in BSE mode.

#### *Bulk microstructure evolution*

After 2958 h at 625 °C, no significant microstructure evolution was noticed for Ti6242S alloy, Figure 5.e. On the contrary, β21s alloy, which was initially single-phased β, exhibited a dual-phased microstructure after 2958 h at 625 °C, Figure 5.f. A similar evolution was observed in the bulk and close to the surface of β21s alloy. Therefore, the microstructure evolution was due to the alloy ageing rather than oxygen diffusion. According to calculations made using Thermo-Calc software with TCTH1 database, composition at equilibrium would be 92.5 % of α and 4.7 % of β for Ti6242S alloy, and 49.5 % of α and 47.7 % of β for β21s alloy (in mol.%). Therefore, the initial β21s microstructure was clearly metastable.

*Micro-hardness*

As oxygen diffused within the Ti-based alloys when exposed to high temperatures, hardness was increased below the oxide scale. Micro-hardness profiles are given in Figure 6 for both alloys oxidized 2958 h at 625 °C. While the micro-hardness affected zone was estimated as being 125 μm thick for Ti6242S, it was around 240 μm thick for β21s alloy.

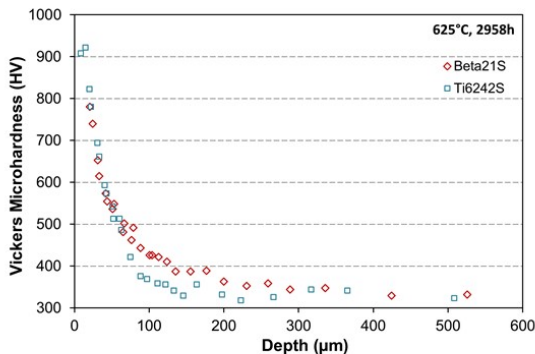


**Figure 6: Micro-hardness profiles of Ti6242S and β21s alloys oxidized for 2958 h at 625 °C under laboratory air.**

*Tensile tests*

Tensile test results on unaged and oxidized specimens of both alloys are presented Figure 7. Three samples per system (not aged or oxidized) were tested. Whatever the alloy, very close engineering stress versus engineering strain curves were obtained for a given system. Besides, the oxidation treatment strongly altered the mechanical behavior of both alloys by reducing drastically the elongation at failure, as already showed [7,8].

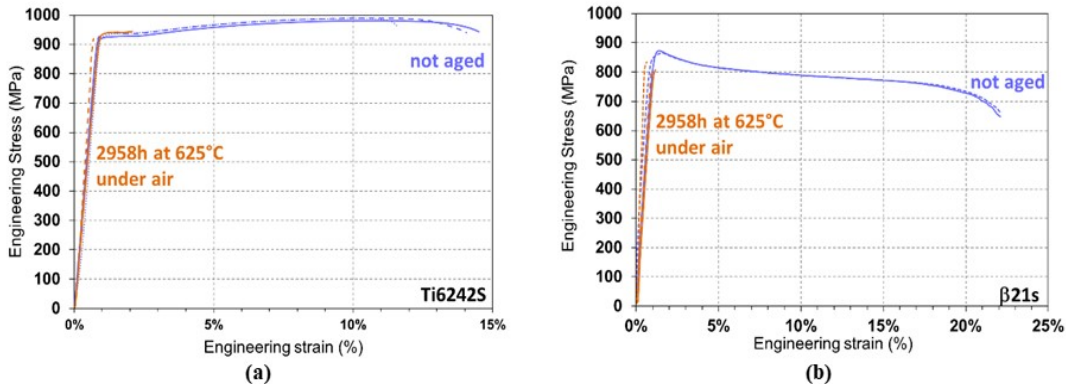


**Figure 7: Engineering stress versus engineering strain for not aged and oxidized (2958 h at 625 °C) (a) Ti6242S and (b) β21s**

Examples of fracture surfaces and microcracks are given for both oxidized alloys after testing with Figures 8 and 9 respectively. Below the oxide scale, the observed fracture surface was typical of a brittle failure. A mixed failure zone was present underneath, and then a fracture surface typical of a ductile behavior. The zone exhibiting a brittle and mixed failure was around 95 μm thick

for Ti6242S alloy and deeper than 370  $\mu\text{m}$  for  $\beta$ 21s alloy (Figure 8). As for microcracks, they were 59  $\mu\text{m}$  long for Ti6242S alloy and 164  $\mu\text{m}$  long in the case of  $\beta$ 21s alloy for which the microcrack spread through the former  $\beta$  grains (Figure 9).

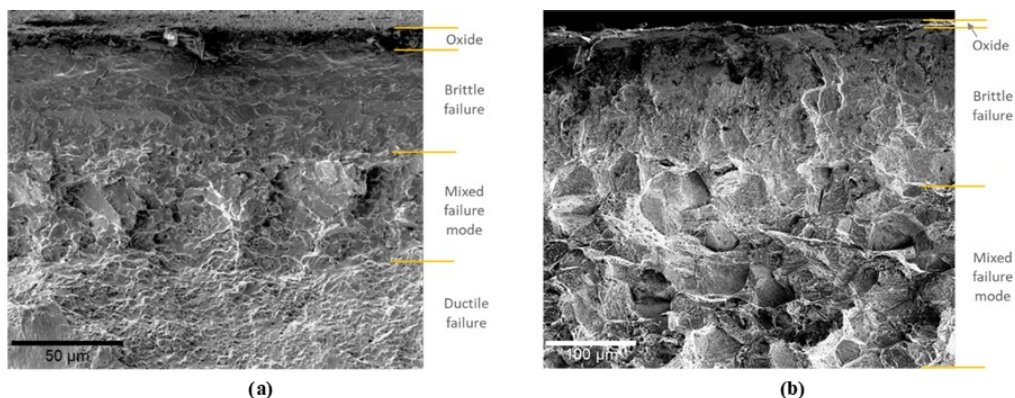


**Figure 8: SEM images, in SE mode, of the fracture of (a) Ti6242S and (b)  $\beta$ 21s specimens after an oxidation of 2958 h at 625 °C and a tensile test**

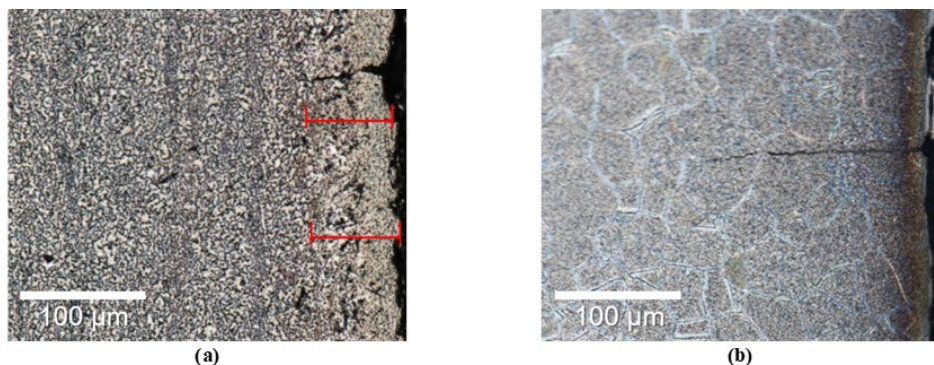


**Figure 9: Optical images of cracks observed on tensile specimens for (a) Ti6242S and (b)  $\beta$ 21s alloys after an oxidation of 2958 h at 625 °C**

#### **4. Discussion**

After 2958 h of oxidation at 625 °C, the overall mass variation, due to oxide formation and oxygen dissolution within the alloy, was 1.3 times much higher for Ti6242S alloy compared to  $\beta$ 21s alloy. Ti6242S and  $\beta$ 21s alloys showed similar oxide scale compositions and close thicknesses. Despite a pronounced microstructure evolution during oxidation,  $\beta$ 21s alloy was richer in  $\beta$  phase than Ti6242S.  $\beta$  phase is known to dissolve much less oxygen than  $\alpha$  (up to 8 at.% and 33.9 at.% for  $\beta$ - and  $\alpha$ -Ti [9]). Therefore, similar or higher mass gains for Ti6242S can only be due to a larger quantity of oxygen dissolved in Ti6242S alloy. Micro-hardness profiles apparently do not confirm this argument and tensile tests showed that the oxidizing treatment decreased more strongly the mechanical resistance of  $\beta$ 21s alloy compared to Ti6242S alloy.

These results can be explained by the microstructure differences between  $\beta$ 21s and Ti6242s alloys. Ti6242S has a higher  $\alpha$  phase volume fraction, therefore it dissolves more oxygen which explains the slightly higher mass gains.  $\beta$ 21S has a lower volume fraction of  $\alpha$  phase, but a continuous network of  $\alpha$  phase nucleates and grows at the former  $\beta$  grain boundaries. These “straight”

pathways of  $\alpha$  phase without  $\beta$  precipitates inside may lead to a rapid oxygen diffusion in depth in  $\beta$ 21s alloy. This  $\alpha$ -phase network can “irrigates” the whole microstructure of  $\beta$ 21s alloy. Nevertheless, as the overall  $\alpha$  phase volume fraction of  $\beta$ 21s is smaller than the one of Ti6242S,  $\beta$ 21s dissolves a smaller mass of oxygen. This deep oxygen diffusion was then responsible for the larger decrease in elongation of the alloy when tested under tensile stresses. Indeed, Porter et al. observed a good agreement between the crack depth compared to the micro-hardness affected zone and the oxygen-rich layer measured after etching [10].

## **5. Conclusions**

Two titanium-based alloys were oxidized between 500 and 625 °C for 2958 h: Ti6242S and  $\beta$ 21s alloys. Samples oxidized at 625 °C were also mechanically tested and compared to non-aged materials. Oxide scale compositions and thicknesses were close but the microstructures were very different between alloys. Ti6242S alloy had an  $\alpha/\beta$  globular microstructure which did not significantly evolved. In the contrary,  $\beta$ 21s microstructure, initially  $\beta$  single-phased, exhibited a basketweave microstructure within the former  $\beta$  grains and a wide  $\alpha$  phase network, imprint of the previous  $\beta$  grain boundaries. Ti6242S alloy showed smaller mass variations than  $\beta$ 21s alloy at 500 and 560 °C. However, it exhibited greater mass variations after 1000 h at 625 °C but its ductility was less decreased than the one of  $\beta$ 21s alloy when tested under tensile stresses after an oxidation of 2958 h at 625 °C. With a similar or lower quantity of oxygen dissolved, ductility of  $\beta$ 21S was more affected by the environment. From the micro-hardness profiles, and from the observation of fracture surfaces and crack lengths, it seems that oxygen diffused deeper in the  $\beta$ 21S alloy. This could be due to the continuous network of  $\alpha$  phase at the former  $\beta$  grain boundaries.

## **6. References**

- [1] C. Leyens and M. Peters, Titanium and Titanium Alloys, Fundamental and Applications, (2003) 532 pages
- [2] G. Lütjering, J. C. Williams, Titanium, Springer Editions (2007) 449 pages
- [3] P. Kofstad, K. Hauffe, H. Kjollesdal, Acta Chemica Scandinavica, 12 (1958) 239-266
- [4] B. Champin, L. Graff, M. Armand et al., Journal of the Less Common Metals, 69 (1980) 163-183
- [5] W.L. Finlay, J.A. Snyder, Journal of Metals, 188 (1950) 227-286.
- [6] H. Fukai, H. Lizumi, K. Minakawa et al., Isij International, 45 (2005) 133-141.
- [7] A. Casadebaigt, D. Monceau, J. Hugues, Proceeding of the 14th World Conference on Titanium, Nantes (France), Juin 10-14, 2019
- [8] D. Texier, Q. Sirvin, V. Velay et al., Proceeding of the 14th World Conference on Titanium, Nantes (France), Juin 10-14, 2019

[9] J.L. Murray, H.A. Wriedt, Bulletin of Alloy Phase Diagrams, 8 (1987) 148-165.

[10] J. Porter, N.D. Schehl, A.L. Pilchak et al., AeroMat25 Conference, June 16-19 (2014) Orlando FL (USA)